Intragraben fault zones and hot-spring deposits in the Oregon-Idaho graben: a geophysical study

Michael L. Cummings, Ansel G. Johnson, and Kenneth M. Cruikshank
Department of Geology, Portland State University, P.O. Box 751, Portland, OR 97207

ABSTRACT

A gravity survey in the central part of the Oregon-Idaho graben indicates high density materials underlie two large paleo hot spring, precious-metals-bearing prospects. The Oregon-Idaho graben is 50 kilometers wide and occurs near the common boundary of the western Snake River plain, Snake River plain, Basin and Range Province, and the western margin of the North American craton. The graben evolved from 15.5 to approximately 10.5 Ma by east-west extension. Intragraben fault zones, including the Wall Rock Ridge (WRRFZ) and Dry Creek Buttes (DCBFZ) fault zones, divided the Oregon-Idaho graben into independently evolving sub-basins that persisted between approximately 14.5 and 12.5 Ma. Sediment-hosted, gold-bearing, hot-spring prospects at Red Butte, Quartz Mountain (Page prospect), and Grassy Mountain developed within 0.5 Ma of peak deformation along the intragraben fault zones. Quartz Mountain occurs within the WRRFZ, Grassy Mountain occurs within the DCBFZ, and Red Butte lies immediately west of the DCBFZ.

Gravity was measured along the 28.5-km Red Butte line that extends west from the shore of Lake Owyhee. The line passes north and west of Red Butte and 8 km south of Quartz Mountain. The east end ends within the DCBFZ, but the line crosses the WRRFZ. Gravity stations are at 200 m spacing.

West of the WRRFZ is a gravity low that extends 11 km to the western end of the line near McNulty Reservoir. Within the DCBFZ gravity decreases near the western edge of the zone, but increases eastward in the last three kilometers toward the Owyhee Reservoir. Beyond the east end of the line are rocks of the Mahogany Mountain and Three Fingers calderas. Between the WRRFZ and DCBFZ is a gravity high of 20 mGal which may be modeled as a slab with a positive density contrast of 0.6 g/cm^3 located at a depth of approximately 2.0 km. The slab is 1.4 km thick and 22 km wide with the eastern margin located in the vicinity of the DCBFZ. Quartz Mountain and Red Butte are hosted in sediments that overlie this intrusion.

INTRODUCTION

The Oregon-Idaho graben (Fig. 1) evolved between 15.5 and 10.5 Ma during east-west rifting near the ancient cratonic boundary of North America. The graben is one segment of a larger middle Miocene rift that extends approximately 1000 km from southern Nevada to southeastern Washington and includes the northern Nevada rift (Zoback et al., 1994), Oregon-Idaho graben (Cummings et al., 1994), Baker and LaGrande basins, and the dike swarms of the Columbia River Basalt Group (Hooper and Swanson, 1990) (Fig. 1).

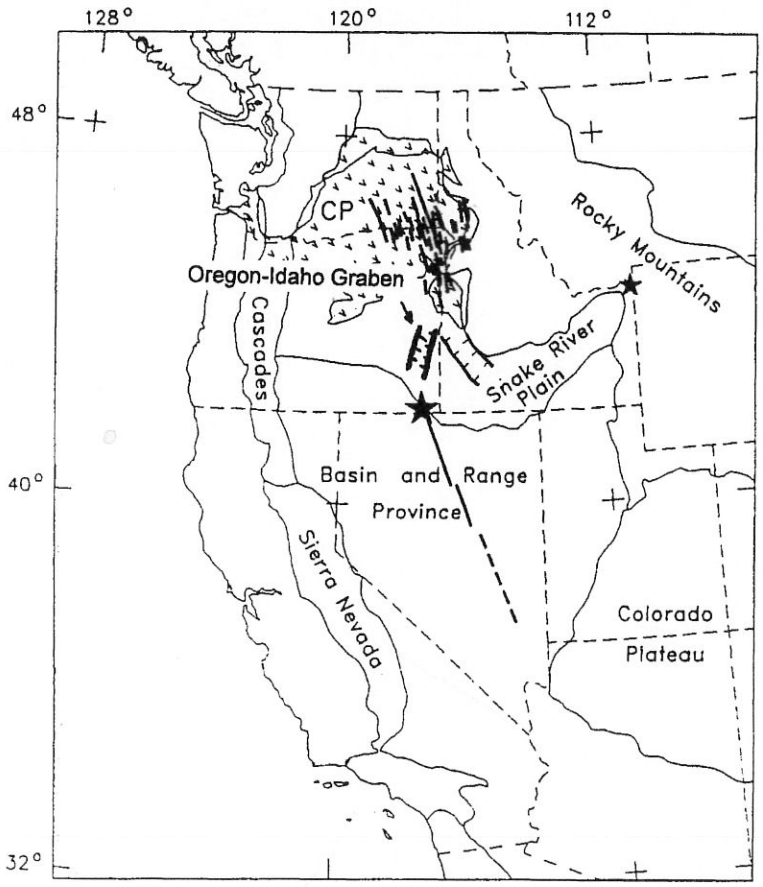

Figure 1—Location of the Oregon-Idaho graben in the context of the middle Miocene rift system in Nevada, Oregon, and Washington. The large star near the Oregon-Nevada border is the McDermitt volcanic field. The small star located in northwestern Wyoming is the present location of the Yellowstone hotspot. Modified from Zoback and others (1994).

Subsidence within the 50 km-wide Oregon-Idaho graben kept pace with accumulation of volcanic and volcaniclastic deposits. Intragraben fault zones were particularly active between 14.3 and 12.6 Ma as the Oregon-Idaho graben divided into independently evolving sub-basins in which locally erupted basalt and basalt hydrovolcanic deposits accumulated along with felsic-dominated volcaniclastic sediments. Periodic incursions of fluviatile sediments from the Idaho batholith region of Idaho produced accumulations of muscovite-bearing arkose and conglomeratic arkose. Large geothermal systems discharging at hot springs along intragraben fault zones formed precious metals-bearing prospects hosted within the clastic and volcaniclastic deposits.

A gravity survey was conducted from the western shore of Lake Owyhee to McNulty Reservoir, 28.5 km to the west. The location of the survey was such that it crosses two intragraben fault zones, the Wall Rock Ridge (WRRFZ) and Dry Creek Buttes (DCBFZ) fault zones, and passes within 2 and 8 km of the hot spring gold prospects located at Red Butte and Quartz Mountain, respectively (Fig. 2). In this paper we summarize the evolution of the Oregon-Idaho graben, present models constructed from gravity data, and discuss the implications of these models for the evolution of the Oregon-Idaho graben and the generation of hot-spring precious metals deposits in this area.

OREGON-IDAHO GRABEN: AN OVERVIEW

The evolution of the Oregon-Idaho graben is summarized by Ferns et al. (1993a,b) and Cummings et al. (1994). The graben developed within a region that experienced widespread tholeiitic basalt volcanism between 17 and 16 Ma as the Columbia River Basalt Group, Steens Basalt, and the basalt of Malheur Gorge (unnamed igneous complex of Kittleman et al., 1965) erupted. Between 15.5 and 15.0 Ma large-volume rhyolitic flows and ash-flow tuffs and tholeiitic basalt to basaltic andesite flows were erupted along the western margin and within the Oregon-Idaho graben. These eruptions coincided with early subsidence of the graben. Named units include the Dinner Creek Ash-Flow Tuff (15.3 Ma), Hunter Creek Basalt (15.78±0.59 to 16.49±1.2 Ma, Lees, 1994), and Littlefield Rhyolite (15.24±0.31 Ma, Lees, 1994) near the western margin of the graben and the Spring Creek and Leslie Gulch ash-flow tuffs (15.4 and 15.5 Ma, respectively, Rytuba and Vander Meulen, 1991) from within the Oregon-Idaho graben. The calderas and ash-flow sheets constitute the Lake Owyhee volcanic field (Rytuba, 1994).

After initial subsidence, the Oregon-Idaho graben developed in three stages (Cummings et al., 1994): 1) widespread deposition of tuffaceous and arkosic fluviatile and lacustrine sediments across the width of the graben (15.5-14.3 Ma); 2) eruptions of calc-alkaline silicic to mafic volcanic rocks from vents aligned along active intragraben fault zones and contemporaneous formation of stratigraphically distinct sub-basins (14.3-12.6 Ma); and 3) waning of faulting and volcanism as sub-basins within the graben were buried by sedimentary sequences (12.6-10.5 Ma).

Three intragraben fault zones have been identified; the Wall Rock Ridge (WRRFZ), Dry Creek Buttes (DCBFZ), and Devils Gate fault zones (DGFZ) (Fig. 2). Intragraben fault zones served as conduits for the ascent of magmas and provided the structural control for geothermal systems during stages 2 and 3. The WRRFZ, DCBFZ and DGFZ also controlled the location of basalt hydrovolcanic vents and distribution of sedimentary facies (Cummings, 1991a,b). Each fault zone is 2 to 3 km wide and characterized by closely spaced, steeply dipping, north-striking normal faults some of which display early down-to-the-east and, subsequent, down-to-the-west senses of displacement (Cummings, 1995). The DCBFZ (Fig. 3) appears to have experienced the greatest displacement for it bounds the western side of a horst block in which rocks of the Mahogany Mountain and Three Fingers calderas and Leslie Gulch and Spring Creek ash-flow tuffs are exposed. The cumulative displacement across this zone may be as great as 1 km.

Intragraben fault zones control the locations of basalt tuff cones (Cummings and Growney, 1988) and sills which are faulted and intruded by dikes. Low-silica rhyolite to rhyodacite volcanic vents are also localized along these intragraben fault zones. These include the vents for the 12.6 Ma tuff of Kern Basin within the DCBFZ (Ferns and Cummings, 1992; Cummings et al., 1994).

Hot-spring deposits

Precious metals-bearing hot spring prospects occur in rocks of the Oregon-Idaho graben. These prospects occur in a variety of rock types including silicified arkosic sandstones (Grassy Mountain, Quartz Mountain, Red Butte, and Shell Rock Butte), rhyolite (Katey East, Freezeout Mountain, Bannock, Hillside, and Double Mountain), basalt (Gold Creek), and hydrovolcanic eruptive centers (Dry Creek Buttes, Mars, and Mahogany). Various aspects of these prospects have been examined by Evans (1986), Gilbert (1988), Evans et al. (1990), Rytuba et al. (1991), Zimmerman (1991), Cummings (1991a), Suchomel et al. (1993), and Zimmerman and Larson (1994).

Alteration within the DCBFZ occurs at several small prospects including the Mars and Dry Creek Buttes prospects which are hosted in basalt hydrovolcanic deposits. Also within the zone is an altered area greater than 2 km^2 formed by a vapor-dominated geothermal system that evolved within the roof of an andesite intrusion during magmatic crystallization (Shickman et al., 1993; Barnes et al., 1993; Savage and Cummings, 1995).

Sediments hosting Grassy Mountain, Quartz Mountain (Page) and Red Butte prospects were deposited during stages 2 and 3 of graben evolution. Large geothermal systems evolved concurrently with high rates of deformation along intragraben fault zones as basalt tephra, flows, and volcaniclastic sediments accumulated. Discharge of fluids from these systems occurred at hot springs located within the WRRFZ at

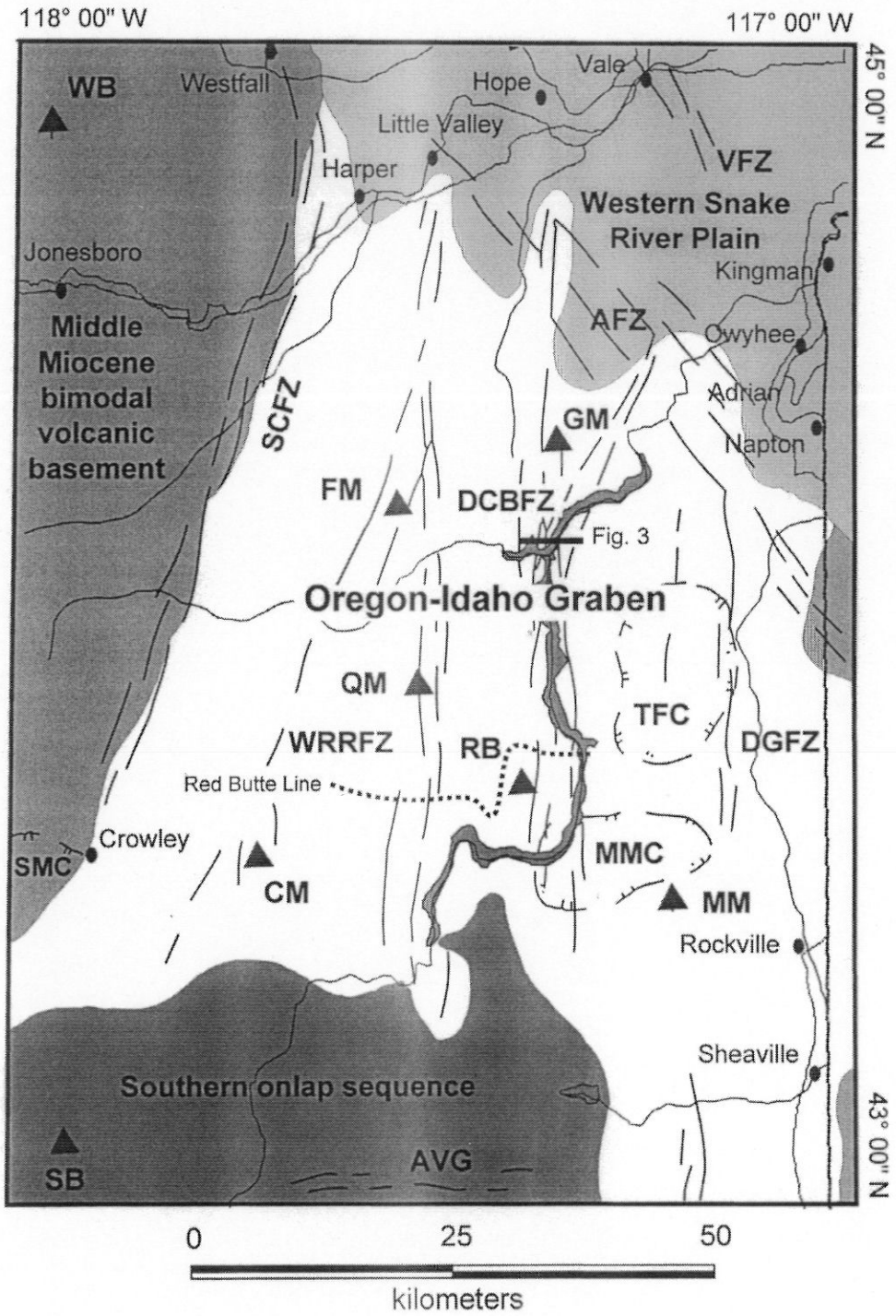

Figure 2—Generalized geologic map of the Oregon-Idaho graben. DCBFZ, Dry Creek Buttes fault zone; WRRFZ, Wall Rock Ridge fault zone; VFZ, Vale fault zone; AFZ, Adrian fault zone; SCFZ, Squaw Creek fault zone; AVG, Antelope Valley graben; MMC, Mahogany Mountain caldera; TFC, Three Fingers caldera; SMC, Star Mountain caldera; WB, Westfall Butte; FM, Freezeout Mountain; QM, Quartz Mountain; RB, Red Butte; GM, Grassy Mountain; CM, Cedar Mountain; SB, Saddle Butte; MM, Mahogany Mountain.

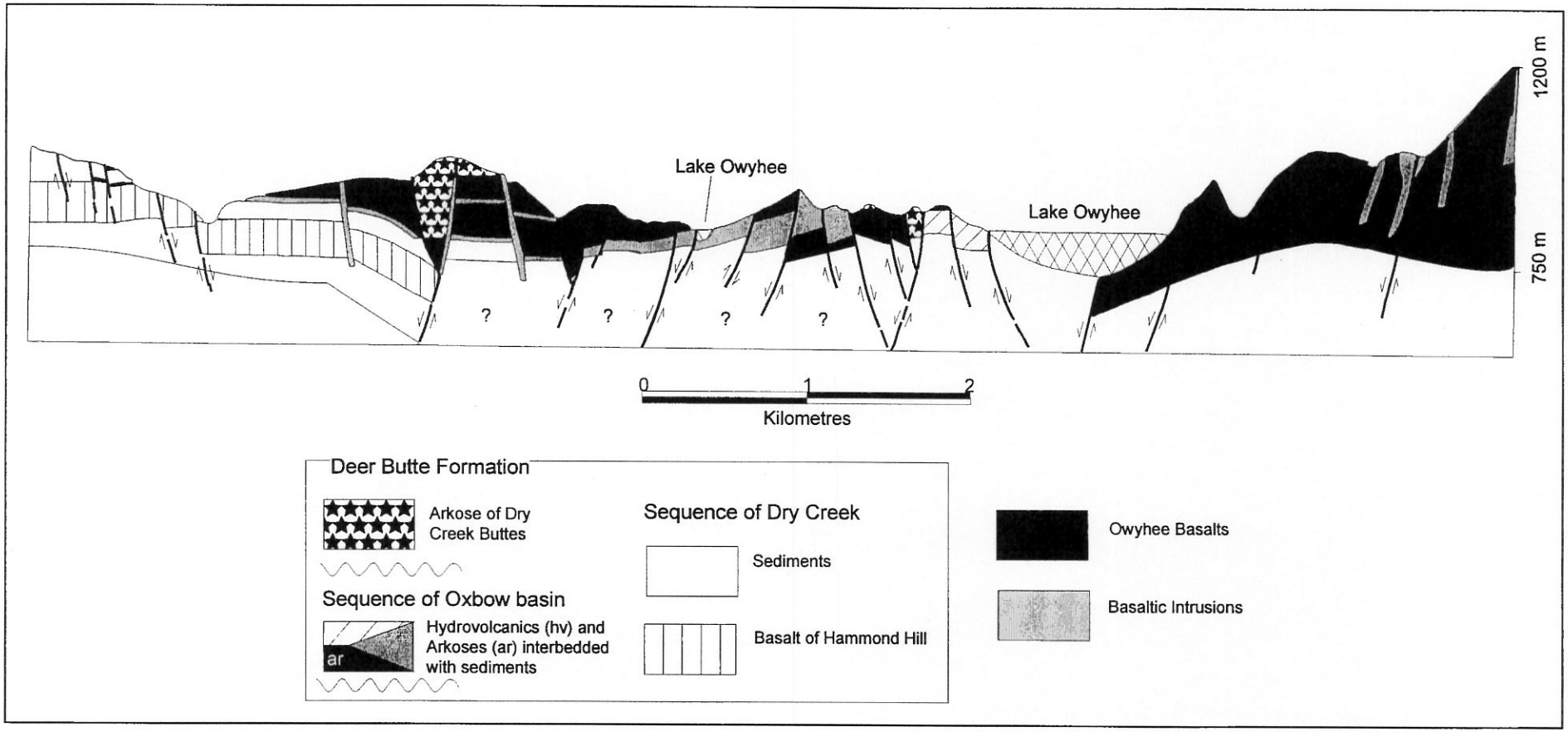

Figure 3—Geologic cross-section across the Dry Creek Buttes Fault Zone (DCBFZ) in the vicinity of the Dry Creek Arm of Lake Owyhee (The Elbow (Ferns and Cummings, 1992), and Twin Springs (Cummings, unpublished mapping, 1988) quadrangles).

Quartz Mountain and the DCBFZ at Grassy Mountain and Red Butte.

Hot spring deposits interbedded with arkosic channel and overbank deposits occur at Grassy Mountain prospect. The arkosic sediments are interbedded with lithic-rich tuffs in the lower part of the Grassy Mountain Formation. A jaw bone from a rhinoceros within the tuff suggests a Barstovian age (16.6-11.2 Ma; Ferns and Ramp, 1989) consistent with a radiometric age determination of 12.6 Ma (Ferns and Cummings, 1992) for a block of flow-banded rhyolite. The Grassy Mountain prospect lies along the western edge of the DCBFZ within 1 to 2 km of exposed rhyolite domes. Reserves are 995,990 ounces gold and 2,467,400 ounces silver (Anonymous, 1992).

The gravity survey was conducted near the Red Butte and Quartz Mountain prospects (Fig. 4). Arkosic and volcaniclastic sediments at the Red Butte and Quartz Mountain prospects are part of the Deer Butte Formation, a stage two sequence. Quartz Mountain lies within the WRRFZ and Red Butte lies 2 km west of the western edge of the DCBFZ. Quartz Mountain is an erosion-resistant ridge capped by silicified and veined, muscovite-bearing arkose and silica sinter. The arkose overlies clay-rich lacustrine volcaniclastic sediments. Northeast of Quartz Mountain (2.8 km) this lacustrine unit contains debris flow deposits that include clasts of silica sinter. The lacustrine sediments overlie the basalt of Hammond Hill, an olivine basalt unit as much as 65 m thick, that originally covered over 350 km^2, and was probably erupted from vents presently buried west of Quartz Mountain.

Hot spring activity began during deposition of the lacustrine sediments and continued as the medium-grained, muscovite-bearing arkose was deposited. Quartz Mountain prospect evolved along an actively deforming fault whereby the accumulating sinter was broken up and shed into the neighboring lake basin by debris flows.

Red Butte is an exceptionally well-exposed paleo-hot spring that lies within the Dry Creek Buttes Wilderness Study Area. Johnson (1961) measured a stratigraphic section on the west flank of the butte and assigned the stratigraphy to various members of the Deer Butte Formation (Kittleman et al., 1965). Evans (1986) determined the alteration patterns and the stratigraphy in the vicinity of Red Butte. Zimmerman (1991) and Zimmerman and Larson (1994) examined alteration patterns in greater detail and determined the oxygen isotopic composition of calcite, quartz, and adularia. Thatcher and Cummings (1994) and Zimmerman and Larson (1994) describe a well-exposed hydrothermal eruption crater located on the southeast flank of the butte.

At Red Butte, the basalt of Hammond Hill is overlain by 40 m of waterlain crystal tuffs and tuffaceous siltstone and mudstone. A thin gravel layer (1 to 3 m thick) containing clasts of rhyolite, basalt, black to dark gray sinter, quartz, and feldspar occurs near the top of the fine-grained sediments. A strongly rooted, leached and oxidized, fossil plant-bearing mudstone overlies the gravel layer and marks the top of the lower sedimentary sequence of the butte. Above this paleosol lies approximately 10 m of cross-bedded sandstone and pebble conglomerate. Gray to black sinter clasts are locally common. Silica sinter containing fossil reed stems is interbedded with the coarse-grained sediments. How deeply the butte was buried prior to exhumation is not known; however, brecciated zeolite and calcite veins cutting brecciated adularia and quartz veins, and zeolitic alteration of deposits in the hydrothermal eruption crater occurred when the paleosurface was higher than the modern butte top and during the waning stages of the geothermal system. We propose that the distribution of vein and alteration assemblages and the telescoped nature of these zones as observed by Evans (1986) and Zimmerman and Larson (1994) reflect hot spring activity keeping abreast of sediment accumulation.

Based on geologic mapping conducted in the summer of 1993 (Cummings, unpublished mapping) and previous studies (Evans, 1986; Zimmerman, 1991; Zimmerman and Larson, 1994) the following evolution of Red Butte is suggested. Hot spring activity commenced, possibly subaqueously, along active faults during deposition of the fine-grained sediments and shortly after eruption of the basalt of Hammond Hill. Construction of sinter deposits and their erosion occurred as the fluvial environment became established. The upper sequence of the butte section accumulated after development of a paleosol. Hot springs discharging into active river channels produced interbedded silica sinter and gravels and erosion of sinter deposits. The environment of deposition at Red Butte is believed similar to that described by Rytuba and Vander Meulen (1991) for the Norris Basin in Yellowstone National Park where hot springs vent through meteoric water-saturated sediments in a small, high-sediment load river. This phase corresponds to the most vigorous hot spring activity, deposition of gold, and excavation and infilling of a hydrothermal eruption crater.

GRAVITY RESULTS

Gravity was measured along the 28.5 km-long Red Butte line that extends from the west bank of the Owyhee Reservoir on the east to McNulty Reservoir on the west (Figure 4). The east end lies within the DCBFZ. From there the line passes 2 km north of Red Butte and crosses the WRRFZ approximately 8 km south of Quartz Mountain. A strip map showing the generalized geology along this line is contained in Figure 4.

Geology along the Red Butte line

The geology along the Red Butte line can be divided into three segments: 1) an eastern segment within the DCBFZ, 2) a central segment extending from the DCBFZ across the WRRFZ, and 3) a western segment extending west of the WRRFZ. These are hereafter referred to as eastern, central, and western segments, respectively.

The eastern segment, within the DCBFZ, is marked by north- and northeast-striking normal faults. The western boundary is defined by a major fault that cuts rocks of the

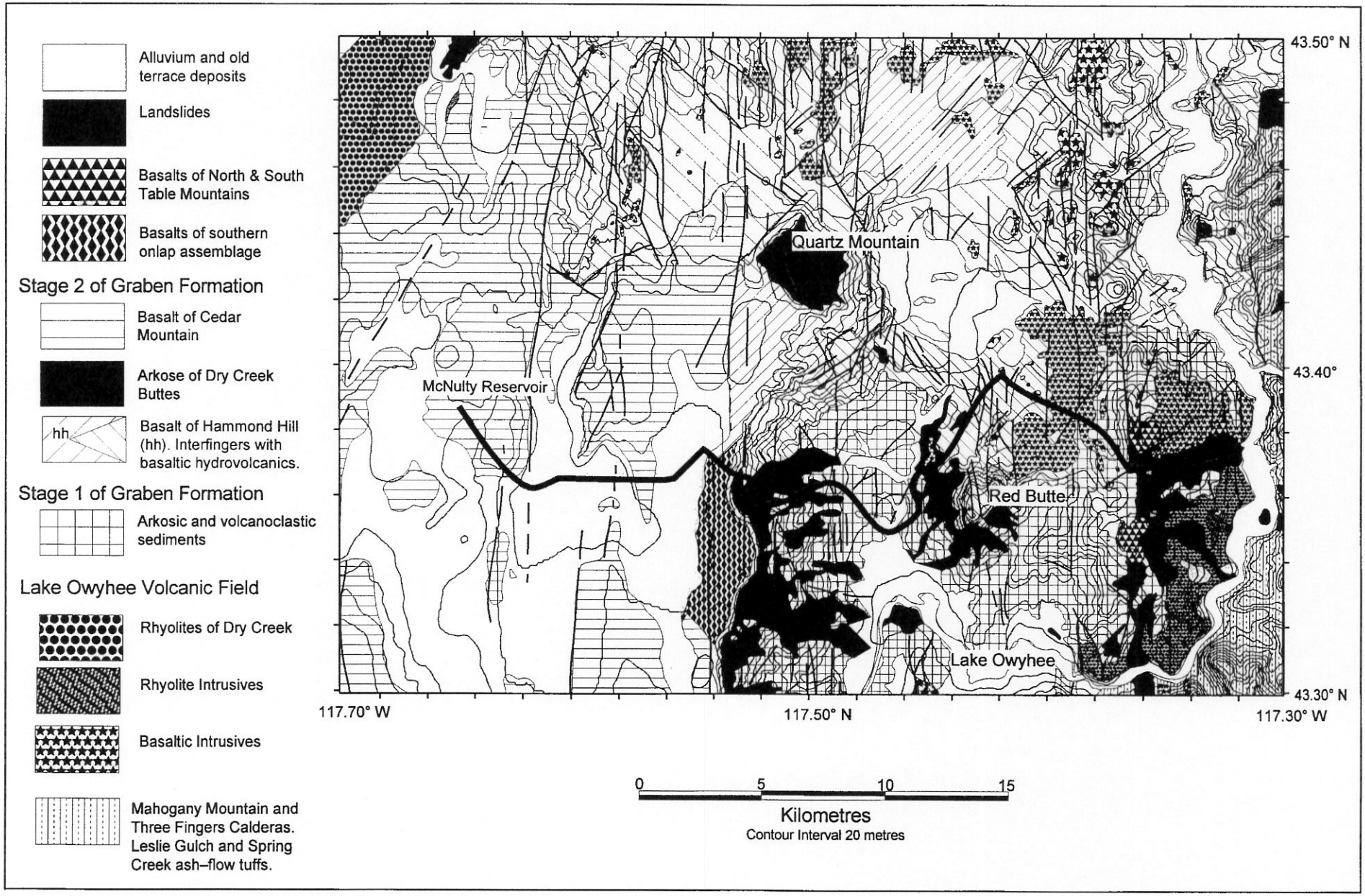

Figure 4—Geologic map in the vicinity of the Red Butte line. Modified from Ferns and others (1993b).

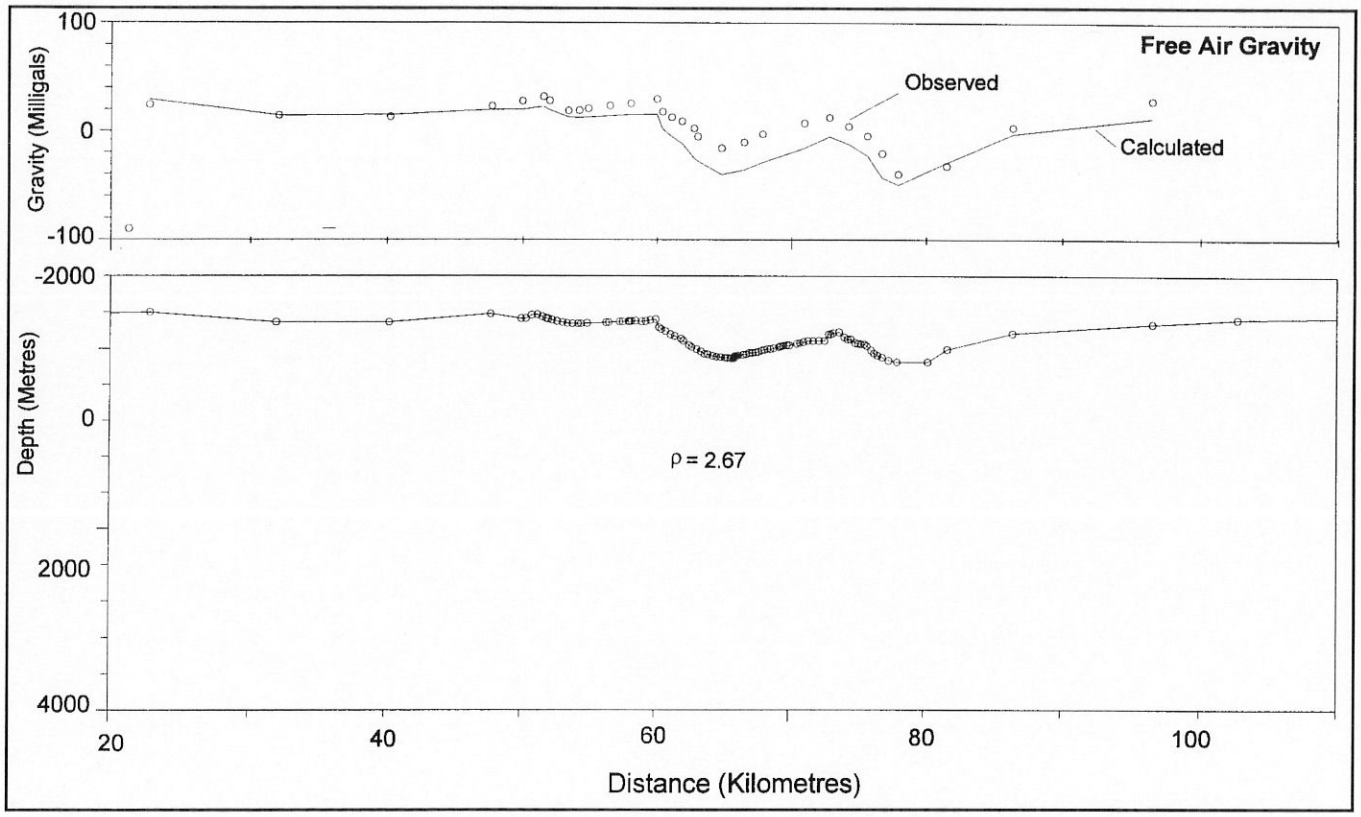

Figure 5—Free Air Gravity model assuming density of 2.67 g/cm³.

Mahogany Mountain caldera to the south. Stage one muscovite-bearing sediments and stage two volcaniclastic sediments and basalt hydrovolcanic deposits make up the stratigraphy within the DCBFZ. These units are intruded by numerous basalt, gabbro, and andesite sills and dikes. Large north- and northeast-trending kink folds have been partially eroded and locally, such as at North Table Mountain, are unconformably overlain by younger basalt flows (Cummings, unpublished mapping, 1993).

The central segment extending from the DCBFZ and across the WRRFZ is underlain by at least 400 m of stage one tuffaceous and arkosic fluviatile sediments. Within the WRRFZ approximately 10 km south of the Red Butte line these sediments are intruded by hornblende dacite(?) intrusions and rhyolite block and ash-flow tuffs are exposed in moderately dipping fault blocks (Cummings, 1992, unpublished mapping).

The western segment is underlain by basalt flows that, in the Big Mud Flat area, are overlain by a thin veneer of sediments. Along the eastern end of this segment the basalt section includes approximately 65 m of the basalt of Hammond Hill and a thin overlying diktytaxitic flow. To the west, the segment is underlain by younger basaltic andesite flows erupted from the Cedar Mountain center. The basalts may overlie volcaniclastic sediments and ash-flow tuffs, a pattern suggested by stratigraphic relations exposed within the WRRFZ (Cummings, 1992, unpublished mapping).

Gravity

Gravity stations were located approximately 200 m apart. Observed gravity was transferred from the airport in Ontario, Oregon where Berg and Thiruvathukal (1965) report a value of 980304.13±0.07 mGal. The Free Air gravity along the Red Butte line for the stations averages near zero suggesting that the area is in isostatic equilibrium.

Gravity models have been developed using a selection of data collected along the Red Butte line and extensions to both the east and west by using data from Hittleman et al. (1994). Three Free Air gravity models for the Red Butte line are presented in Figures 5, 6, and 7. In each case, the model is fixed at a gravity station from Hittleman and others (1994) located approximately 20 km west of McNulty Reservoir, the westernmost gravity station on the Red Butte line. The densities used for different lithologic associations are indicated in Table 1. The gravity data for all stations are presented in Appendix 1 and are available on the Home Page of the Department of Geology (http://www.geol.pdx.edu).

The model in Figure 5 assumes a density of 2.67 g/cm³, average crustal density. In general, the observed gravity mimics

Table 1—Density values and inferred lithologies used to construct gravity models in Figures 6 and 7.

Assumed density value	Lithology
2.85 g/cm^3	Basalt flows including basalt of Hammond Hill and Cedar Mountain. Thin layers of sediments overlie basalts in Big Mud Flat.
2.60 g/cm^3	Volcaniclastic sediments including siltstone, claystone, and fine-grained sandstone. Local basalt hydrovolcanic deposits. May include ash-flow tuffs at depth.
3.20 g/cm^3	Gabbro intrusion
2.75 g/cm^3	Intermediate to granitic intrusions beneath the Mahogany Mountain caldera.
2.67 g/cm^3	Crustal Density

topography, but the measured gravity is substantially higher than the calculated gravity in the central and eastern segments. The calculated model shows a relative deficiency of density in the central and eastern segments of the Red Butte line which require densities greater than 2.67 g/cm^3 to fit the observed gravity data.

The model in Figure 5 was modified by adding blocks of differing densities to obtain the best fit between observed and calculated gravity and remain faithful to the surficial geology. Two such models are presented in Figures 6 and 7. In both cases, a relatively high density mass (3.20 g/cm^3) is included. Figure 6 places this mass at the shallowest position while Figure 7 places it at its greatest depth. In both cases, the calculated gravity matches the observed gravity by incorporating this feature beneath a lower density mass (2.60 g/cm^3) and leaving average crustal density to the west and a required slightly elevated density rock (2.75 g/cm^3) to the east. In both models a thin block of 2.85 g/cm^3 material is placed in the near surface environment of the western segment to account for the thick basalt flows known to be in this area. The thickness and cross sectional area of the high density mass increases steadily as the feature is moved to greater depth. In Figure 7, the depth to the top of the block is approximately 2.0 km, length is 20 km, and thickness is 1.4 km. Placing the block at different depths does not appreciably shift the eastern end of the block from beneath Lake Owyhee and the eastern margin of the DCBFZ. The western edge of the block extends to near the western end of the Red Butte line, but thins west of the approximate location of the WRRFZ.

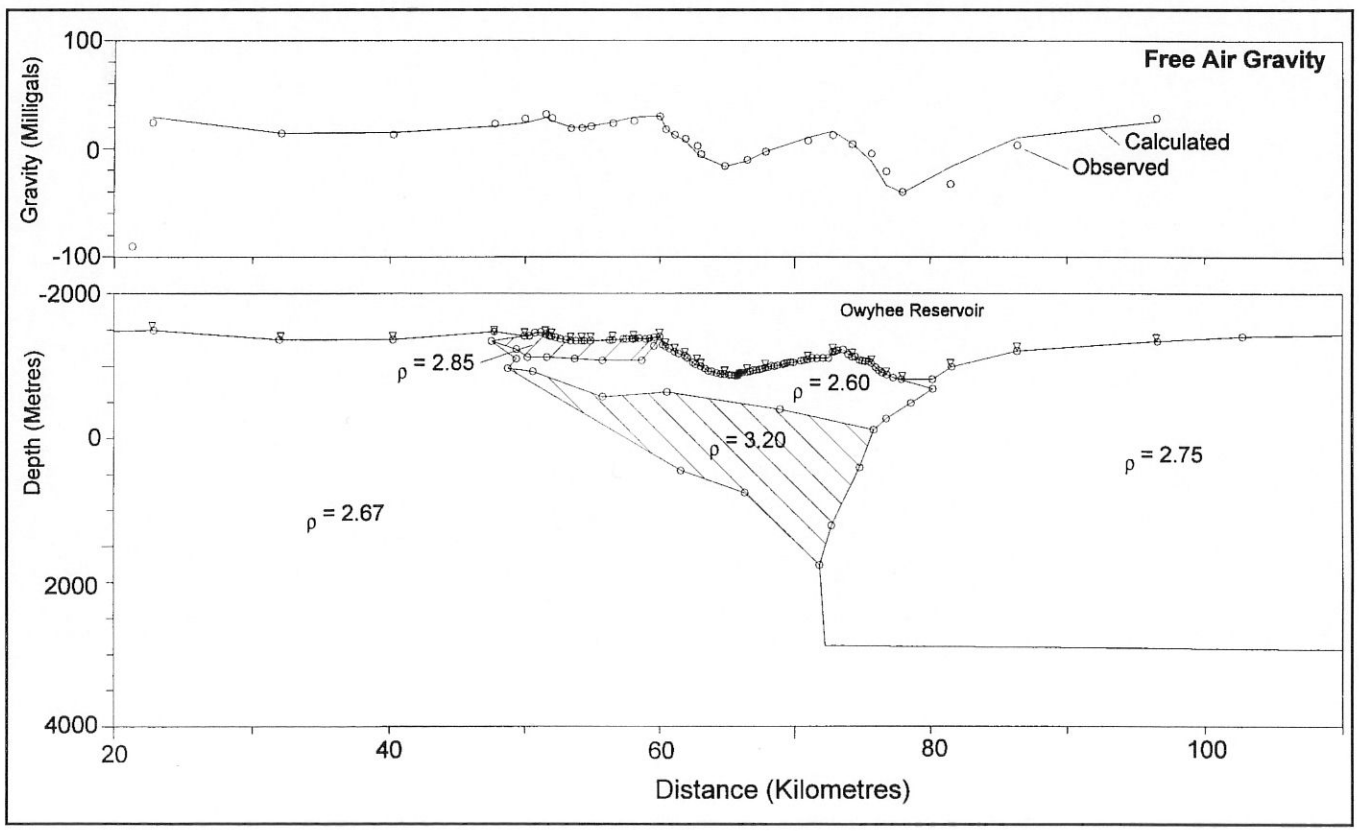

Figure 6—Free Air Gravity model assuming a shallow intrusion.

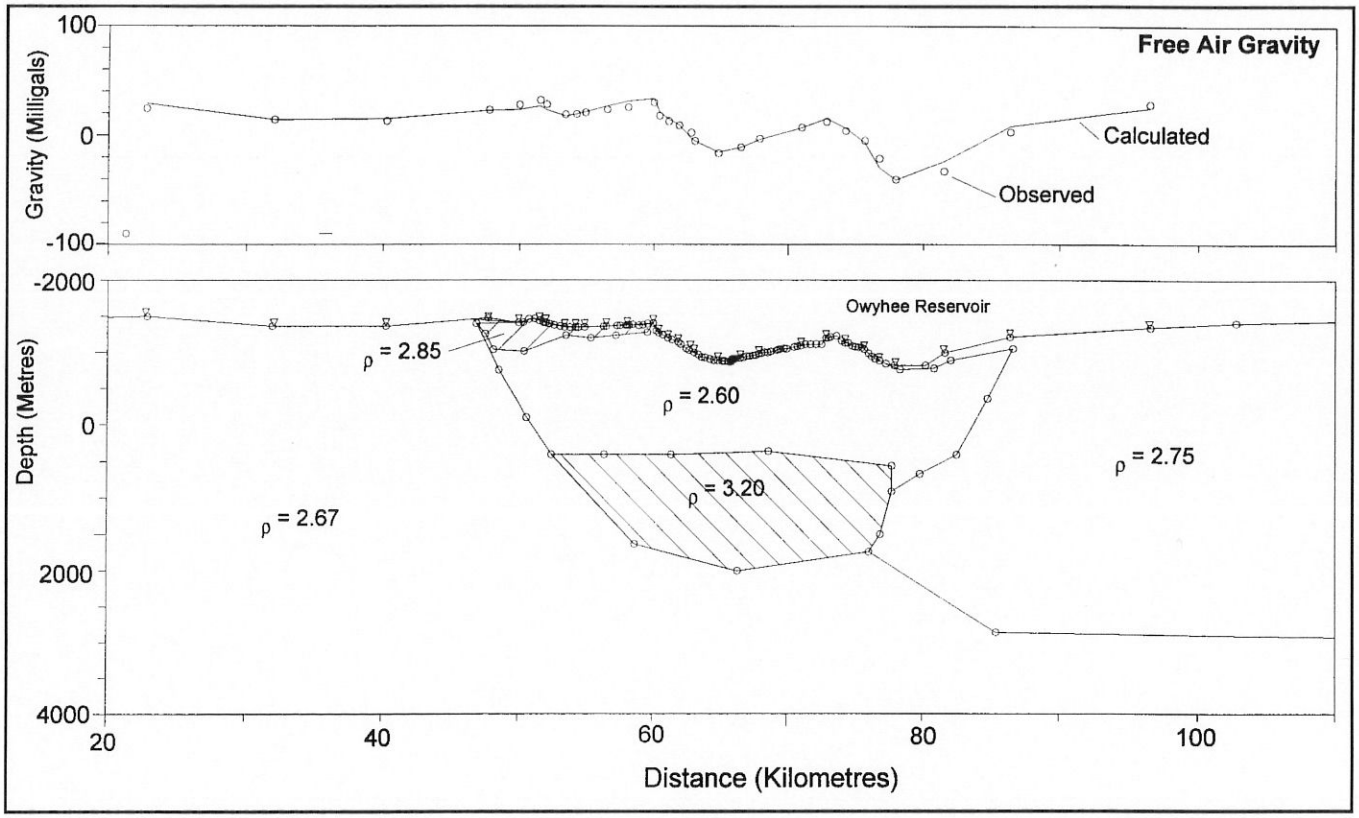

Figure 7—Free Air Gravity model assuming a deep intrusion.

DISCUSSION

The Red Butte line crosses two major fault zones that played an important role in the evolution of the central portion of the Oregon-Idaho graben. The Wall Rock Ridge (WRRFZ) and Dry Creek Buttes (DCBFZ) fault zones host major hot-spring gold prospects. In this discussion 1) the geophysical data are compared to regional data, 2) the geophysical models are reconciled with the geology along the Red Butte line, and 3) the implications of the geophysical and geologic models for evolution of the hot-spring gold deposits are considered.

Regional Gravity Patterns

Figures 8 and 9 indicate the Free Air and Bouguer Gravity, respectively, in the vicinity of the Red Butte line incorporating the new data. The major features are the 20 mGal Bouguer Gravity high west of Lake Owyhee and the 10 mGal Bouguer Gravity low east of the lake. The eastern low is elongated north-south and has a diameter of about twenty-five kilometers. This low coincides with the location of the Three Fingers and Mahogany Mountain calderas (Rytuba, 1994). To the east, another boundary is indicated by the transition from the gravity low to the level of background gravity, -120 mGal. The high to the west is circular, with a diameter of about thirty kilometers. This high extends northward beyond the boundary of the map in Figure 9. The three intragraben fault zones, WRRFZ, DCBFZ, and DGFZ coincide with areas of highest gravity gradients; the most pronounced occurs in the vicinity of the DCBFZ.

Gravity and Geology along the Red Butte Line

Gravity along the three segments of the Red Butte line fails to match the surface geology. The gravity low in the western segment occurs where basalts are exposed and the gravity high in the central segment occurs within an area underlain by sediments.

Although basalt flows are exposed along the western segment (Fig. 4), this segment is likely underlain by volcaniclastic sediments and basalt hydrovolcanic deposits exposed in the canyon of Dry Creek, 7 km north, and at The Hole in the Ground along the canyon of the Owyhee River, 12 km south of the Red Butte line. These materials are underlain by rhyolite flows and domes north of Dry Creek and rhyolite ash-flow tuffs in the vicinity of the Owyhee River. In Figures 6 and 7, this segment is modeled with basalt (2.85 g/cm^3) over materials with average density of 2.67 g/cm^3. The gravity profile is relatively featureless for this 11 km-long segment. The section below the basalt may contain relatively thick sediments overlying rhyolitic rocks. A caldera cannot be ruled

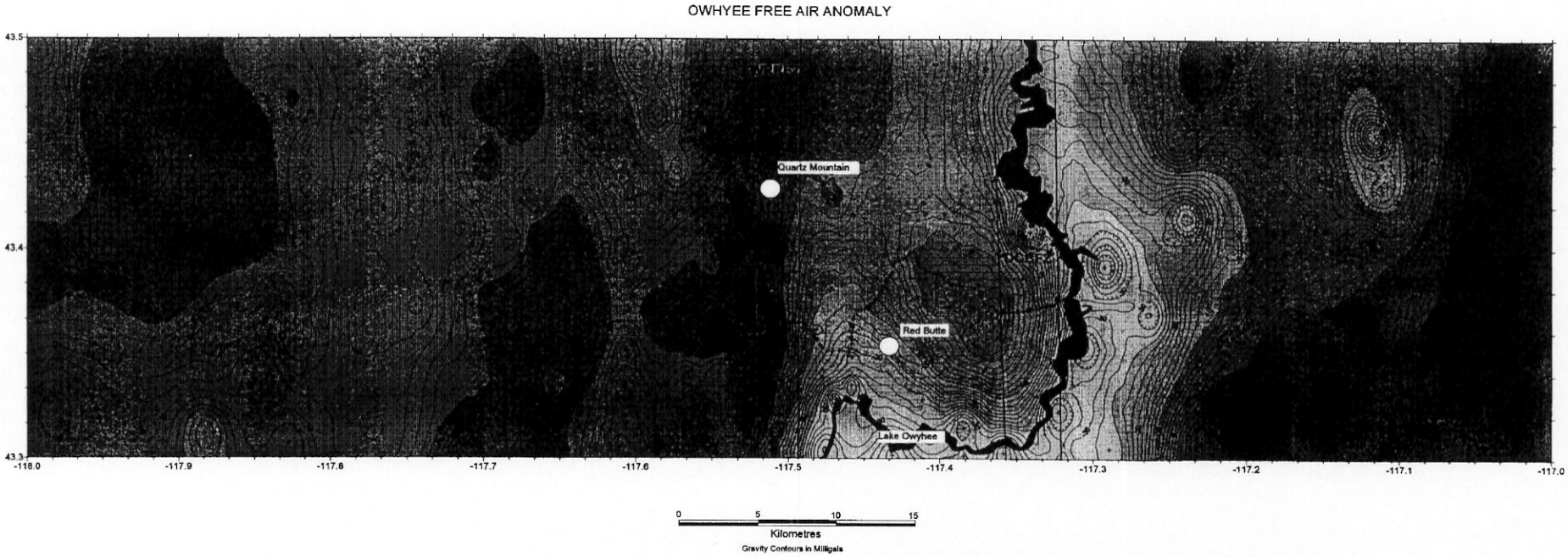

Figure 8—Free Air Gravity map of the Red Butte area between 118° West and 117° West Longitude.

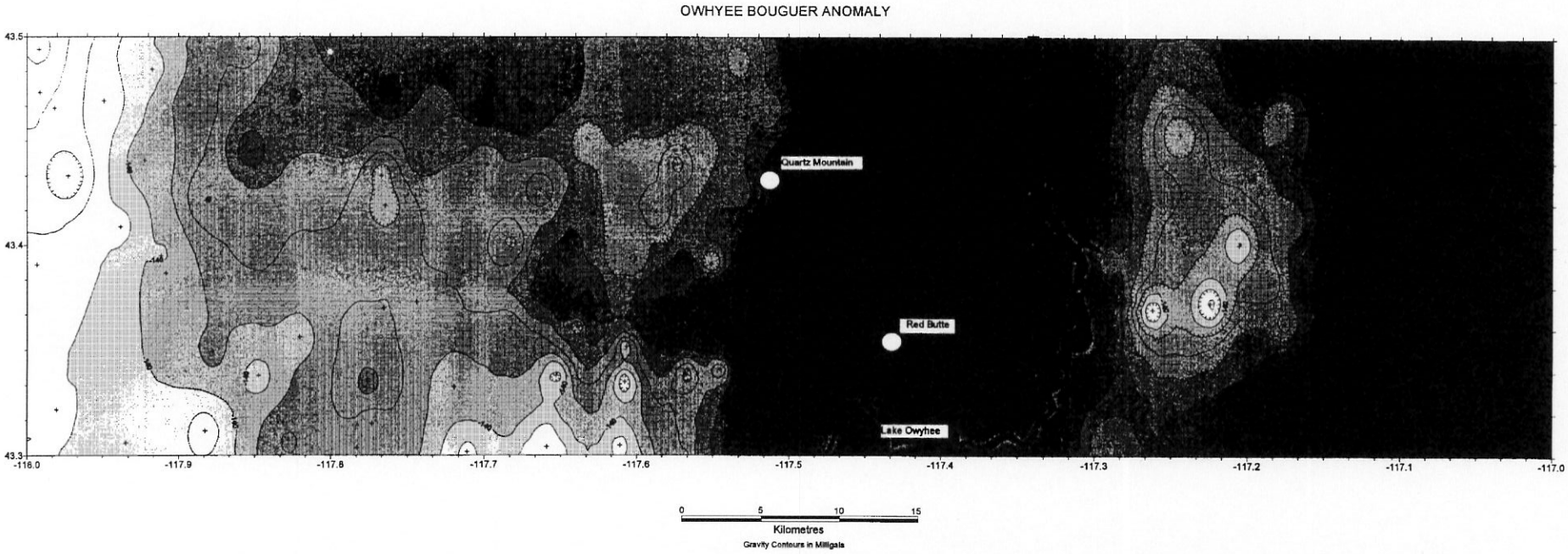

Figure 9—Bouguer Anomaly map of the Red Butte area between 118° West and 117° West Longitude.

out; however, if present, there appears to be no distinct gravity signature.

Volcaniclastic sediments overlying rhyolite ash-flow tuffs, including Leslie Gulch Ash-Flow Tuff and the tuff of Birch Creek (Ferns et al., 1993b), dominate the eastern and central segments, an area where gravity is 20 mGal higher than in the western segment. In Figures 6 and 7 relatively low density rocks (2.60 g/cm^3) overlie high density material (3.20 g/cm^3). The high density material, modeled as a mafic intrusion, intruded along the DCBFZ and spread out west of the fault zone. Exposed sills may have been emplaced over the roof of this intrusion as observed above intrusions along the west shore of Lake Owyhee (Cummings, unpublished mapping, 1993). Basalt sills may extend northward from the Red Butte line and account for the Bouger Gravity anomaly high that dominates the central portion of the Oregon-Idaho graben (Fig. 9). Abundant orthopyroxene-bearing gabbro xenoliths in an andesite intrusion exposed at the south end of Dry Creek Buttes, 12 km north of the Red Butte line (Savage and Cummings, in preparation) are consistent with this interpretation.

Relation to Hot-Spring Precious Metal Deposits

Cummings (1991a,b, 1995) and Cummings et al. (1994) note that the intragraben fault zones within the Oregon-Idaho graben played an important role in localizing geothermal systems within the graben. Timing of large-scale fluid migration occurred between about 13.5 and 12.5 Ma, an apparent thermal maximum coincident with the maximum rate of deformation along the WRRFZ and DCBFZ. Gravity data indicates that this thermal event may have coincided with emplacement of a large mafic intrusion that drove hot springs at Red Butte and Quartz Mountain.

A heat-flow model based on a mafic intrusion was developed to test whether such a mass could produce a thermal anomaly of great enough magnitude and duration to form the hot spring prospects at Red Butte and Quartz Mountain. Figure 10 is a conductive heat flow model that illustrates the maximum temperature within the mafic intrusion as a function of time for the two gravity models presented in Figures 6 and 7. The heat flow model provides a maximum cooling time without convective heat flow. The volume of the intrusion is crudely estimated from 1) the size of the Bouguer gravity anomaly and 2) distribution of inclusions of mafic plutonic rocks in basalt units. Assuming dimensions of 30 km north-south length, 22 km east-west width, and 1.4 km thickness (Fig. 7), the sill's volume is approximately 900 km^3. In comparison, Henley and Ellis (1983) estimated the heat released at the Wairaki geothermal system in New Zealand is equivalent to cooling a 700 km^3 basalt intrusion over a period of 300,000 years. The temperature profile within the intrusion is extremely sensitive to the depth of emplacement as illustrated in Figure 10. The depth shown in Figure 7 is the maximum depth for the intrusion consistent with gravity data. For this configuration, the heat flow from cooling of the intrusion is within the range estimated at 10^5 and 10^6 years for the duration of large geothermal systems (Henley and Ellis, 1983).

Age control is not great enough to rigorously evaluate age relations at Red Butte and Quartz Mountain. However, the sedimentary and volcanic deposits associated with these prospects were deposited between about 14.3 Ma, the most reasonable age for the Owyhee Basalt (Cummings et al., 1994), and the eruption of the tuff of Kern Basin at 12.6 Ma (Ferns and Cummings, 1992). Although age determinations are not available for the basalt of Hammond Hill, stratigraphic data indicate that hot spring activity at Red Butte and Quartz Mountain began at approximately the same time, shortly following eruption of the basalt of Hammond Hill. Although it is tempting to argue that the basalt of Hammond Hill was erupted during sill emplacement, there are no data that support this speculation.

Rytuba (1994) emphasizes cooling of large batholiths intruded during eruption of the Lake Owyhee volcanic field between 15.5 and 15.0 Ma as playing an important role in mineralization. Although this is a reasonable hypothesis, Red Butte and Quartz Mountain are both located above what we interpret as a large mafic intrusion capable of accounting for the Bouguer Gravity high located west of Lake Owyhee and having enough heat to produce geothermal systems that operated for at least 10^5 years, long enough to mineralize these prospects.

CONCLUSIONS

1) Evolution of precious-metal-bearing hot spring systems was intimately associated with the thermal and structural evolution of the Oregon-Idaho graben. Fluid migration leading to mineralization occurred along intragraben fault zones during the second and third stage of

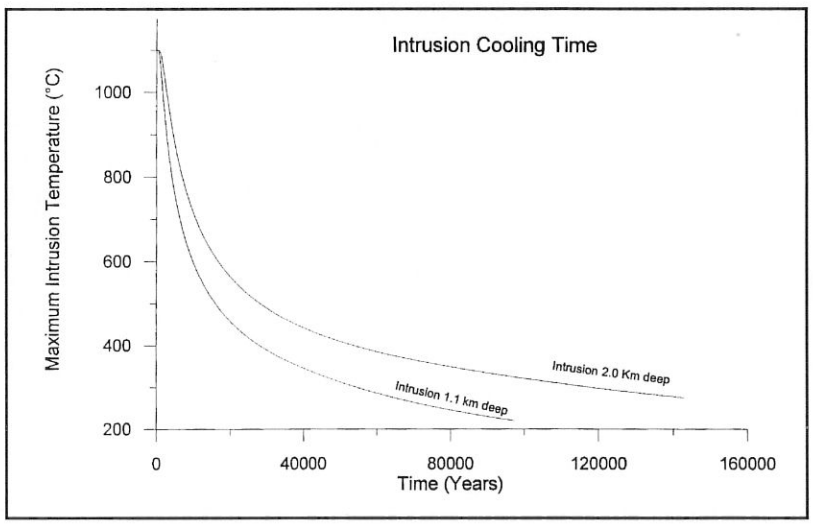

Figure 10—Heat flow models for cooling of a mafic intrusion located at depths indicated in Figures 6 and 7.

graben evolution while intragraben fault zones were particularly active.

2) The gravity profile along the Red Butte line does not reflect the surface geology. Basalt flows occur where gravity is low while sediments crop out within a gravity high.
3) The gravity model that most closely summarizes known geology and provides the best fit between observed and calculated gravity places a gabbro intrusion at a depth greater than 2.0 km. The cross section of this intrusion is 1.4 km by 22 km. The intrusion may have been intruded along the DCBFZ and spread laterally to the west.
4) Coeval evolution of the Red Butte and Quartz Mountain prospects occurred along the DCBFZ and WRRFZ, respectively. The geothermal systems responsible for these prospects evolved during cooling of a mafic intrusion.

REFERENCES

Anonymous, 1992, The Mining Record, 1992, Denver, Colorado, v. 103, no. 9, p. 31.

Barnes, M., Cummings, M., Shickman, K., and Neidig, S., 1993, Geology of a vapor-dominated, fossil geothermal system: Owyhee Uplands, Malheur County, Oregon: Geological Society of America Abstracts with Programs, v. 25, no. 5, p. 6.

Berg, J. W., Jr., and Thiruvathukal, J. V., 1965, Gravity base station network, Oregon: Journal of Geophysical Research, v. 70, p. 3325-3330.

Cummings, M. L., and Growney, L.P., 1988, Basalt hydrovolcanic deposits in the Dry Creek arm area of the Owyhee Reservoir, Malheur County, Oregon: Stratigraphic relations: Oregon Geology, v. 50, no. 7/8, p. 75-82, 94.

Cummings, M. L., 1991a, Geology of the Deer Butte Formation, Malheur County, Oregon: Faulting, sedimentation, and volcanism in a post-caldera setting, *in*, R. Cas and C. Busby-Spera, eds., Volcaniclastic Sedimentation, Sedimentary Geology, v. 74, p. 345-362.

Cummings, M. L., 1991b, Relations among volcaniclastic sedimentation, volcanism, faulting, and hydrothermal activity west of Lake Owyhee, Malheur County, Oregon, *in*, Raines, G., Lisle, R. E., Schafer, R. W., and Wilkinson, W. H., eds., Geology and ore deposits of the Great Basin: Geological Society of Nevada Symposium Proceedings, v. 1, p. 111-132.

Cummings, M. L., Ebeling, C., and Johnson, A. G., 1993, North-striking fault zones and evolution of the central graben, Ore-Ida graben, Malheur County, Oregon: Geological Society of America Abstracts with Programs, v. 25, no. 6, p. 26.

Cummings, M. L., Evans, J. G., and Ferns, M. L., 1994, Stratigraphic and structural evolution of the middle Miocene Oregon-Idaho graben, Malheur County, Oregon, *in* D. A. Swanson and R. S. Haugerud, editors, Geologic field trips in the Pacific Northwest: 1994 Geological Society of America Annual Meeting, p. 1G1-1G20.

Cummings, M. L., 1995, Intragraben fault zones, volcanism, and geothermal evolution in the Oregon-Idaho graben, U.S.A., *in*, J. L. Mauk and J. D. St. George, editors, PACRIM Contress 1995, Exploring the Rim, The Australasian Institute of Mining and Metallurgy Publication Series No. 9/95, p.169-174.

Evans, C. S., 1986, The geology, geochemistry, and alteration of Red Butte, Oregon: A precious metal-bearing paleo hot spring system: M.S. thesis, Portland, Oregon: Portland State University, 133 p.

Evans, J. G., Frisken, J. G., Griscom, A., Sawatsky, D. L., and Miller, M. S., 1990, Mineral resources of the Gold Creek and Sperry Creek Wilderness Study Areas, Oregon: U.S. Geological Survey Bulletin 1741-E, 20 p.

Ferns, M. L. and Ramp, L., 1989, Geology and Mineral Resources Map of the Grassy Mountain quadrangle, Malheur County, Oregon: Oregon Department of Geology and Mineral Industries Geological Map Series, GMS-57, scale 1:24,000.

Ferns, M. L. Brooks, H. C., Evans, J. G., Cummings, M. L., 1993a, Geologic map of the Vale 30 × 60 minute quadrangle, Malheur County, Oregon, and Owyhee County, Idaho: Oregon Department of Geology and Mineral Industries Geologic Map Series GMS-77, scale 1:100,000.

Ferns, M. L., and Cummings, M. L., 1992, Geology and mineral resources map of The Elbow quadrangle, Malheur County, Oregon: Oregon Department of Geology and Mineral Industries Geological Map Series GMS-62, scale 1:24,000.

Ferns, M. L., Evans, J. G., Cummings, M. L., 1993b, Geologic map of the Mahogany Mountain 30 × 60 minute quadrangle, Malheur County, Oregon, and Owyhee County, Idaho: Oregon Department of Geology and Mineral Industries Geologic Map Series GMS-78, scale 1:100,000.

Gilbert, D., 1988, Geology and geochemistry of the Mahogany hot-springs gold prospect in the Owyhee region of southeastern Oregon: M.S. thesis, Seattle, Washington: University of Washington, 76 p.

Henley, R. W. and Ellis, A. J., 1983, Geothermal systems ancient and modern: a geochemical review: Earth-Science Reviews, v. 19, p. 1-50.

Hittleman, A., D. Dater, R. Buhmann, and S. Racey, Gravity CD-ROM and User's Manual (1994 Edition), National Oceanic and Atmospheric Administration, National Geophysical Data Center, Boulder, Colorado.

Hooper, P. L. and Swanson, D. A., 1990, The Columbia River Basalt Group and associated volcanic rocks of the Blue Mountains Province, *in* G. W. Walker, ed., Geology of the Blue Mountains region of Oregon, Idaho, and Washington: Cenozoic geology of the Blue Mountains Region: U.S. Geological Survey Professional Paper 1437, p. 63-99.

Johnson, A., 1961, Stratigraphy and lithology of the Deer Butte Formation, Malheur County, Oregon: MS thesis, Eugene Oregon: University of Oregon, 75 p.

Kittleman, L. R., Green, A. R., Hagood, A. R., Johnson, A. M., McMurray, J. M., Russell, R. G., and Weeden, D. A., 1965, Cenozoic stratigraphy of the Owyhee region, southeastern Oregon: Eugene, Oregon University of Oregon Museum of Natural History Bulletin 1, 45 p.

Lees, K. R., 1994, Magmatic and tectonic changes through time in the Neogene volcanic rocks of the Vale area, Oregon, north western USA: Ph.D. dissertation, The Open University, 284 p.

Rytuba, J. J., and Vander Meulen, D. B., 1991, Hot-spring precious-metal systems in the Lake Owyhee volcanic field, Oregon-Idaho, *in*, Raines, g., Lisle, R. E., Schafer, R. W., and Wilkinson, W. H., eds., Geology and ore deposits of the Great Basin: Geological Society of Nevada, Symposium Proceedings, v. 2, p. 1085-1096.

Rytuba, J. J., Vander Meulen, D. B., and Barlock. V. E., 1991, Tectonic and stratigraphic controls on epithermal precious metal mineralization in the northern part of the Basin and Range, Oregon, Idaho, and Nevada, *in* J. J. Rytuba, D. B. Vander Meulen, V. E. Barlock, and M. L. Ferns, Field guide to hot-spring gold deposits in the Lake Owyhee volcanic field, eastern Oregon: Geological Society of Nevada and U. S. Geological Survey Field Trip No. 10, p. 1-15.

Rytuba, J. J., 1994, Evolution of volcanic and tectonic features in caldera settings and their importance in the localization of ore deposits: Economic Geology, v. 89, p. 1687-1696.

Savage, K. S. and Cummings, M. L., 1995, Mass-balance calculations and water-rock ratios in an altered andesitic intrusion, Acton Gulch, Owyhee Uplands, Malheur County, Oregon: Geological Society of America Abstracts with Programs, v. 27, no. 5, p. 76.

Shickman, K. S., Barnes, M., and Cummings, 1993, Alteration chemistry and mineralogy of an andesitic intrusion, Owyhee Uplands, Malheur County, Oregon, v. 25, no. 5, p. 146.

Suchomel, B. J., Taufen, P. M., and Marvin, R. D., 1993, The combined use of structural analysis and ultra-low detection limit soil and stream-sediment geochemistry to discover concealed high-grade gold mineralization at Freezeout Mountain, Malheur County, Oregon:

Thatcher, S. K. and Cummings, 1994, Evolution of a gold-bearing hot spring at Red Butte, Malheur County, Oregon: Hydrothermal explosion crater: Proceedings of the Oregon Academy of Science, v. XXX, p. 33.

Zimmerman, B. S., 1991, Geology and geochemistry of epithermal gold mineralization in the Lake Owyhee volcanic field-western Snake River plain region of eastern Oregon and western Idaho: Ph.D. dissertation: Pullman, Washington, Washington State University, 262 p.

Zimmerman, B. S. and Larson, P. B., 1994, Epithermal gold mineralization in a fossil hot spring system, Red Butte, Oregon: Economic Geology, v. 89, p. 1983-2002.

Zoback, M. L., McKee, E. H., Blakely, R. J., and Thompson, G. A., 1994, The northern Nevada rift: Regional tectono-magmatic relations and middle Miocene stress direction: Geological Society of America Bulletin, v. 106, p. 371-382.

Recommended citation:
Cummings, M.L., Johnson, A.G., and Cruikshank, K.M., 1996, Intragraben fault zones and hot-spring deposits in the Oregon-Idaho graben: a geophysical study, *in* Coyner, A.R., and Fahey, P.L., eds., Geology and Ore Deposits of the American Cordillera: Geological Society of Nevada Symposium Proceedings, Reno/Sparks, Nevada, April 1995, p. 1047-1062.

Appendix 1—Gravity Data West of Owyhee Lake

Geology Department, Portland State University

Station number	Latitude (degrees)	Measured Gravity (mgals)	Terrain Correction (mgals)	Elevation (metres)	Latitude (degrees)	Free Air (mgals)	Bouguer (mgals)
1	43.35333	980180.61	1.55	903.86	117.47750	-10.6012	-110.17
2	43.35444	980178.79	1.61	911.69	117.47894	-10.105	-110.50
4	43.35694	980177.32	1.67	919.53	117.48075	-9.38109	-110.59
5	43.35888	980176.80	1.72	924.35	117.48188	-8.58834	-110.28
6	43.35916	980175.95	1.81	925.47	117.48248	-9.11603	-110.84
8	43.36111	980175.09	1.90	932.44	117.48520	-8.0048	-110.43
9	43.36194	980172.03	1.98	945.44	117.48746	-7.12523	-110.91
10	43.36333	980165.87	2.01	966.47	117.48830	-6.92215	-113.04
11	43.36500	980161.75	2.04	976.24	117.48950	-8.17424	-115.35
12	43.36500	980158.35	2.07	996.48	117.49222	-5.33158	-114.75
14	43.36500	980154.79	2.10	1026.93	117.49698	0.502699	-112.29
15	43.36416	980149.28	2.12	1050.73	117.49939	2.412043	-113.02
16	43.36361	980142.55	2.15	1079.24	117.50196	4.534413	-114.06
17	43.36250	980133.71	2.18	1114.69	117.50467	6.727872	-115.80
18	43.36194	980127.98	2.20	1139.15	117.50611	8.596501	-116.65
19	43.36166	980127.21	2.22	1142.63	117.50679	8.925246	-116.69
20	43.36083	980122.79	2.24	1157.78	117.50905	9.2632	-118.03
21	43.36055	980118.90	2.26	1177.31	117.51034	11.42267	-118.03
22	43.35972	980119.26	2.22	1175.91	117.51283	11.42076	-117.91
23	43.35888	980116.07	2.19	1187.52	117.51464	11.89322	-118.77
24	43.35833	980113.32	2.16	1198.93	117.51660	12.71034	-119.26
25	43.35805	980111.78	2.13	1205.50	117.51902	13.22955	-119.51
26	43.35750	980105.72	2.16	1231.10	117.52022	15.11647	-120.45
27	43.35722	980102.48	2.20	1244.97	117.52128	16.18139	-120.91
28	43.35694	980099.65	2.23	1256.40	117.52294	16.9046	-121.43
29	43.35777	980096.09	2.26	1270.92	117.52506	17.74826	-122.17
30	43.35805	980089.47	2.31	1295.47	117.52747	18.68353	-123.94
31	43.35944	980085.04	2.36	1318.06	117.52898	21.10109	-124.00
32	43.36083	980080.26	2.55	1338.05	117.52958	22.35658	-124.79
33	43.36194	980080.31	2.80	1337.06	117.52981	22.00446	-124.78
34	43.36388	980075.54	2.46	1361.71	117.52958	24.66448	-125.22
35	43.36500	980069.88	2.41	1389.39	117.52951	27.44336	-125.59
37	43.36611	980067.37	2.55	1404.97	117.53034	29.64876	-124.98
38	43.36666	980067.79	2.16	1403.47	117.53313	29.54707	-125.31
39	43.35166	980180.21	1.58	889.92	117.47380	-15.1491	-113.13
40	43.35166	980179.77	1.62	887.72	117.47010	-16.2744	-113.97
41	43.35166	980181.79	1.66	878.18	117.46618	-17.2008	-113.79
42	43.35166	980182.37	1.69	876.24	117.46369	-17.2178	-113.56
43	43.35138	980184.89	1.94	862.30	117.46014	-18.9668	-113.50
44	43.35305	980183.80	1.82	867.86	117.46006	-18.4973	-113.77
45	43.35472	980183.82	2.08	870.27	117.45795	-17.8782	-113.16
46	43.35638	980182.88	2.19	877.20	117.45765	-16.8329	-112.78
47	43.35722	980182.27	1.74	873.86	117.45803	-18.5565	-114.59
48	43.35833	980183.35	2.07	870.97	117.45818	-18.4666	-113.84
49	43.36000	980181.21	1.96	880.00	117.45765	-17.9636	-114.45
50	43.36250	980181.92	1.62	889.63	117.45712	-14.5102	-112.42
51	43.36305	980180.39	1.85	897.08	117.45772	-13.7931	-112.31
52	43.36416	980181.45	1.55	893.64	117.45871	-13.8902	-112.32
53	43.36666	980179.37	1.48	905.31	117.45674	-12.6009	-112.41
54	43.36833	980179.54	1.40	907.00	117.45591	-12.0539	-112.12
55	43.37083	980179.27	1.44	909.50	117.45357	-11.7865	-112.10

Appendix 1—Gravity Data West of Owyhee Lake (continued)

Geology Department, Portland State University

Station number	Latitude (degrees)	Measured Gravity (mgals)	Terrain Correction (mgals)	Elevation (metres)	Latitude (degrees)	Free Air (mgals)	Bouguer (mgals)
56	43.37111	980178.07	1.49	915.28	117.45146	-11.2259	-112.13
57	43.37111	980177.54	1.54	918.55	117.44927	-10.7434	-111.97
58	43.37194	980176.64	1.59	924.42	117.44761	-9.91295	-111.74
59	43.37305	980177.12	1.64	925.09	117.44640	-9.32681	-111.18
60	43.37388	980176.13	1.56	930.78	117.44504	-8.6267	-111.20
61	43.37444	980173.41	1.48	944.73	117.44338	-7.09407	-111.31
62	43.37611	980174.65	1.40	940.06	117.44165	-7.45126	-111.22
63	43.37694	980174.02	1.36	943.44	117.44067	-7.11153	-111.30
64	43.37805	980171.05	1.32	955.78	117.43991	-6.37538	-111.99
65	43.37972	980172.29	1.28	950.78	117.43870	-6.8268	-111.92
66	43.38055	980171.87	1.23	954.05	117.43757	-6.31411	-111.82
67	43.38222	980171.32	1.18	957.48	117.43621	-5.9504	-111.89
68	43.38416	980170.75	1.13	960.18	117.43508	-5.86233	-112.16
69	43.38527	980169.55	1.07	967.78	117.43417	-4.81966	-112.02
70	43.38638	980170.24	1.02	966.94	117.43342	-4.49253	-111.65
71	43.38750	980167.97	1.09	979.24	117.43221	-3.06196	-111.52
72	43.38916	980169.53	1.06	973.41	117.43078	-3.45664	-111.30
74	43.39222	980168.66	1.13	980.05	117.43048	-2.55171	-111.07
75	43.39361	980168.29	1.03	984.25	117.42957	-1.75062	-110.84
76	43.39416	980168.00	0.92	987.19	117.42844	-1.18389	-110.71
77	43.39444	980164.54	0.82	1003.34	117.42678	0.312824	-111.12
78	43.39527	980166.65	0.71	995.83	117.42413	0.033454	-110.67
79	43.39638	980168.70	0.62	998.20	117.42255	2.705988	-108.35
80	43.39722	980165.87	0.53	1010.06	117.42119	3.460809	-109.01
81	43.39833	980163.99	0.44	1021.57	117.41968	5.036693	-108.81
82	43.39861	980163.65	0.44	1023.89	117.41613	5.389276	-108.72
83	43.39777	980162.75	0.44	1026.69	117.41538	5.423956	-109.00
84	43.39583	980159.71	0.44	1037.77	117.41523	5.982461	-109.68
85	43.39416	980159.35	0.44	1037.79	117.41462	5.78297	-109.88
86	43.39277	980158.26	0.44	1039.78	117.41379	5.428032	-110.45
87	43.39166	980158.23	0.45	1042.65	117.41236	6.382557	-109.81
88	43.39055	980156.21	0.46	1045.84	117.41002	5.448552	-111.10
89	43.39027	980154.64	0.47	1054.49	117.40896	6.570243	-110.94
90	43.38916	980154.56	0.48	1049.82	117.40662	5.151853	-111.82
91	43.38861	980152.62	0.49	1056.83	117.40466	5.431645	-112.32
92	43.38805	980150.45	0.50	1063.96	117.40202	5.509367	-113.03
93	43.38750	980148.32	0.51	1072.51	117.39975	6.068009	-113.42
94	43.38777	980148.08	0.52	1074.80	117.39885	6.505623	-113.22
95	43.38694	980148.75	0.53	1073.98	117.39741	7.002941	-112.62
96	43.38638	980146.51	0.55	1081.36	117.39696	7.085073	-113.35
97	43.38500	980144.79	0.56	1086.25	117.39485	6.999143	-113.97
98	43.38361	980142.27	0.58	1094.60	117.39334	7.188312	-114.69
99	43.38333	980141.07	0.60	1103.21	117.39130	8.667688	-114.16
100	43.38277	980139.10	0.62	1110.55	117.38926	9.013699	-114.61
101	43.38250	980139.06	0.64	1109.37	117.38722	8.630735	-114.84
102	43.38222	980139.44	0.68	1109.07	117.38466	8.941281	-114.46
103	43.38250	980136.05	0.72	1122.50	117.38141	9.674139	-115.19
104	43.38194	980137.13	0.76	1112.42	117.37922	7.688487	-116.00
105	43.38111	980136.55	0.80	1109.91	117.37696	6.414974	-116.96
106	43.38000	980136.41	1.03	1110.39	117.37424	6.520127	-116.68
107	43.37916	980136.18	1.25	1110.85	117.37303	6.508038	-116.52

Appendix 1—Gravity Data West of Owyhee Lake (continued)

Geology Department, Portland State University

Station number	Latitude (degrees)	Measured Gravity (mgals)	Terrain Correction (mgals)	Elevation (metres)	Latitude (degrees)	Free Air (mgals)	Bouguer (mgals)
108	43.37888	980132.25	1.48	1124.70	117.37326	6.877759	-117.47
109	43.37833	980130.03	1.71	1136.07	117.37333	8.21946	-117.17
110	43.37805	980127.47	1.68	1145.00	117.37318	8.440906	-117.98
111	43.37694	980123.92	1.65	1157.45	117.37273	8.832138	-119.01
112	43.37472	980117.41	1.62	1187.12	117.37175	11.68022	-119.51
113	43.37361	980114.23	1.59	1199.41	117.37024	12.38751	-120.21
114	43.37166	980114.40	1.70	1200.10	117.36820	12.94705	-119.61
115	43.36916	980111.03	1.82	1213.04	117.36609	13.80017	-120.09
116	43.37083	980107.64	1.93	1224.35	117.36345	13.74758	-121.29
117	43.37055	980105.72	2.05	1228.38	117.36058	13.09745	-122.28
118	43.37027	980115.09	1.98	1184.16	117.35839	8.844215	-121.66
119	43.37000	980120.05	1.91	1159.95	117.35575	6.36338	-121.50
120	43.37027	980126.38	1.84	1131.92	117.35258	4.014805	-120.79
121	43.37027	980125.88	1.76	1131.27	117.34986	3.316845	-121.48
122	43.37027	980130.02	1.69	1111.98	117.34820	1.502715	-121.22
123	43.37055	980135.98	1.61	1085.08	117.34578	-0.86491	-120.65
124	43.37111	980138.88	1.53	1073.80	117.34314	-1.49259	-120.10
125	43.37138	980140.30	1.45	1068.68	117.34042	-1.67611	-119.79
126	43.37138	980140.11	1.56	1066.95	117.33710	-2.39847	-120.21
127	43.37166	980145.18	1.66	1042.68	117.33499	-4.84927	-119.84
128	43.37250	980150.46	1.77	1022.62	117.33310	-5.83634	-118.48
129	43.37305	980158.50	1.88	982.15	117.33091	-10.3295	-118.33
130	43.37333	980166.77	1.88	940.43	117.32820	-14.9639	-118.29
131	43.37361	980167.16	1.89	939.67	117.32721	-14.8358	-118.07
132	43.37416	980173.96	1.89	909.11	117.32495	-17.5118	-117.33
133	43.37527	980181.10	1.90	874.67	117.32140	-21.1028	-117.06
134	43.37555	980185.14	2.09	836.56	117.31914	-28.8506	-120.35
135	43.37555	980189.15	2.28	829.44	117.31665	-27.0391	-117.55
136	43.36722	980070.09	1.77	1396.13	117.53532	29.53796	-124.89
137	43.36750	980071.68	1.38	1388.18	117.53728	28.64979	-125.27
138	43.36861	980073.00	0.99	1380.64	117.53962	27.54635	-125.93
139	43.37000	980074.11	0.92	1374.96	117.54136	26.76997	-126.14
140	43.37111	980074.34	0.85	1373.01	117.54332	26.29975	-126.46
141	43.37277	980074.16	0.77	1374.03	117.54513	26.28414	-126.66
142	43.37388	980073.23	0.70	1380.29	117.54755	27.18452	-126.54
143	43.37555	980072.51	0.66	1383.20	117.54921	27.21357	-126.87
144	43.37500	980072.06	0.63	1383.84	117.55110	27.00588	-127.19
145	43.37305	980072.31	0.59	1380.29	117.55276	26.33839	-127.49
146	43.37166	980072.92	0.55	1374.75	117.55442	25.36172	-127.89
147	43.37055	980072.24	0.54	1376.07	117.55570	25.19423	-128.22
148	43.37000	980072.49	0.52	1375.08	117.55744	25.18815	-128.13
149	43.36888	980072.80	0.51	1372.61	117.55978	24.83713	-128.22
150	43.36805	980072.31	0.49	1372.33	117.56099	24.33628	-128.70
151	43.36680	980072.16	0.47	1371.81	117.56204	23.60446	-129.40
152	43.36555	980071.64	0.45	1371.38	117.56393	23.59436	-129.38
153	43.36555	980071.99	0.43	1371.38	117.56589	23.94529	-129.05
154	43.36583	980073.36	0.41	1366.26	117.57035	23.71644	-128.73
155	43.36583	980074.57	0.43	1361.22	117.57382	23.37238	-128.49
156	43.36555	980075.08	0.44	1358.67	117.57646	23.11859	-128.44
157	43.36555	980076.19	0.46	1352.55	117.58099	22.33333	-128.52
158	43.36555	980076.19	0.42	1351.01	117.58318	21.86011	-128.87

Appendix 1–Gravity Data West of Owyhee Lake (continued)

Geology Department, Portland State University

Station number	Latitude (degrees)	Measured Gravity (mgals)	Terrain Correction (mgals)	Elevation (metres)	Latitude (degrees)	Free Air (mgals)	Bouguer (mgals)
159	43.36555	980075.85	0.37	1349.02	117.58582	20.91243	-129.64
160	43.36555	980075.75	0.32	1349.48	117.58846	20.95261	-129.70
161	43.36555	980075.62	0.27	1348.92	117.59141	20.65257	-129.99
162	43.36555	980075.33	0.27	1349.66	117.59397	20.58739	-130.14
163	43.36555	980074.92	0.26	1347.90	117.59661	19.63833	-130.90
164	43.36555	980074.84	0.26	1347.18	117.59978	19.33342	-131.12
165	43.36555	980074.58	0.26	1347.18	117.60227	19.07291	-131.39
166	43.36555	980074.49	0.30	1347.18	117.60484	18.98144	-131.44
167	43.36555	980074.29	0.34	1347.18	117.60763	18.77651	-131.61
168	43.36555	980073.95	0.38	1348.40	117.60990	18.81349	-131.66
169	43.36527	980073.27	0.42	1350.11	117.61246	18.69448	-131.94
170	43.36472	980072.45	0.42	1356.29	117.61496	19.82933	-131.49
171	43.36416	980071.02	0.41	1362.72	117.61669	20.43052	-131.61
172	43.36333	980069.52	0.41	1368.53	117.61911	20.80273	-131.89
173	43.36277	980068.18	0.41	1376.02	117.62205	21.82145	-131.71
174	43.36333	980066.64	0.42	1386.89	117.62447	23.58653	-131.16
175	43.36388	980066.21	0.42	1393.09	117.62643	25.01945	-130.41
176	43.36527	980065.31	0.42	1401.90	117.62832	26.71534	-129.70
177	43.36583	980064.24	0.43	1409.61	117.62990	27.97278	-129.30
178	43.36722	980063.09	0.43	1418.02	117.63201	29.29418	-128.92
179	43.36888	980061.92	0.46	1426.43	117.63435	30.56817	-128.55
180	43.37083	980059.15	0.49	1440.19	117.63571	31.86746	-128.76
181	43.37166	980056.60	0.53	1451.89	117.63745	32.85556	-129.05
182	43.37305	980053.06	0.56	1466.78	117.64017	33.78528	-129.76
183	43.37388	980050.74	0.59	1475.55	117.64190	34.09614	-130.39
184	43.37527	980052.12	0.53	1470.07	117.64432	33.65156	-130.28
185	43.37694	980054.30	0.47	1460.57	117.64538	32.75109	-130.18
186	43.37888	980057.37	0.42	1447.36	117.64651	31.57296	-129.94
187	43.38194	980064.15	0.36	1414.70	117.65051	27.99796	-129.92
188	43.38388	980066.88	0.30	1401.27	117.65292	26.40746	-130.06
189	43.38555	980065.89	0.24	1404.81	117.65398	26.3561	-130.57
190	43.38750	980064.74	0.18	1413.18	117.65496	27.61039	-130.31